





## Article

# Influence of Powder Plasticity on Bonding Strength of Cold-Sprayed Copper Coating

Fu-Jun Wei <sup>1,2,\*</sup> , Bang-Yen Chou <sup>2</sup> , Kuan-Zong Fung <sup>1</sup>, Shu-Yi Tsai <sup>3</sup>  and Chung-Wei Yang <sup>4</sup> <sup>1</sup> Department of Materials Science and Engineering, National Cheng Kung University, Tainan 70101, Taiwan<sup>2</sup> Department of Research and Development, Plus Metal Tech Co., Ltd., Tainan 71247, Taiwan<sup>3</sup> Hierarchical Green-Energy Materials (Hi-GEM) Research Center, National Cheng Kung University, Tainan 70101, Taiwan<sup>4</sup> Department of Materials Science and Engineering, National Formosa University, Yunlin 63201, Taiwan

\* Correspondence: this.is.fjwei@gmail.com

**Abstract:** When cold spraying is performed at a velocity equivalent to or greater than a specific material-dependent critical velocity, powders suffer intensive plastic deformation and localized heating of interacting surfaces. The thermomechanical reaction of the sprayed powder upon impacting the substrate material triggers thermally dependent metallurgical bonding and/or mechanical interlocking mechanisms. In this study, three Cu feedstocks, fabricated through electrolysis (EP), gas-assisted water atomization (WA), and inert gas atomization (GA), were characterized and annealed before cold spraying. The electron back-scattered diffraction technique was used to analyze the grain structure and plastic microstrain within the powders and coatings. The plastic microstrains that originally existed in the Cu powders were released after 30 min of annealing at 500 °C. The influence of plastic deformation behavior (associated with the grain structure and plastic microstrain of powder feedstocks) on the bonding strength of the cold-sprayed Cu coatings on AA6061 aluminum alloy substrates was examined. The results indicate that EP powder with an asymmetric dendrite morphology was not conducive to the intensive plastic deformation that may cause recrystallized twin grains to form after cold spraying. Furthermore, the homogeneous microstructure of the spherical Cu feedstocks, which may be induced by strain release as recrystallized twin grains and low-angle boundary grain growth through annealing, caused the cold-sprayed Cu coating to have high ductility and low hardness. The findings reveal the low strain hardening and residual stress in the cold-sprayed coating—characteristics regarded as providing key advantages for the bonding strength of the coating.

**Keywords:** cold spray; plastic deformation; strain; recrystallization; bonding strength

**Citation:** Wei, F.-J.; Chou, B.-Y.; Fung, K.-Z.; Tsai, S.-Y.; Yang, C.-W. Influence of Powder Plasticity on Bonding Strength of Cold-Sprayed Copper Coating. *Coatings* **2022**, *12*, 1197. <https://doi.org/10.3390/coatings12081197>

Academic Editor: Yasutaka Ando

Received: 22 July 2022

Accepted: 15 August 2022

Published: 17 August 2022

**Publisher's Note:** MDPI stays neutral with regard to jurisdictional claims in published maps and institutional affiliations.



**Copyright:** © 2022 by the authors. Licensee MDPI, Basel, Switzerland. This article is an open access article distributed under the terms and conditions of the Creative Commons Attribution (CC BY) license (<https://creativecommons.org/licenses/by/4.0/>).

## 1. Introduction

Cold spraying is a technology that is more than two decades old, and it has attracted considerable attention in both academia and industry. In contrast to magnetron sputtering deposition with a thickness of several micrometers [1], cold spray deposition can attain a thickness up to several centimeters [2]. Cold spraying is a rapid kinetic deposition process in which feedstock powders are accelerated to high velocities ranging from 300 to 1200 m/s in a supersonic jet of compressed inert gas, which is preheated to a temperature exceeding 300 °C [2,3]. Upon impacting a substrate, sprayed powders deform in a solid state at temperatures below their melting point. Cold spraying is thus highly suitable for preparing oxidation-sensitive coatings [4]. At a velocity that is equivalent to or greater than a specific material-dependent critical velocity, powders suffer intensive plastic deformation and localized heating of the interacting surfaces because of the aforementioned impact [5–7]. Adiabatic shear instability (i.e., thermal mechanical reaction at an impact interface), which results from the high-strain-rate deformation processes of the powder sample, is believed to cause a localized increase in temperature. The increasing temperature may lead to

the formation of metallurgical bonding and dynamic recrystallization, and it may also cause viscous flow, which leads to the formation of a metal jet comprising powder and substrate materials and contributes to mechanical interlocking [6,8–10]. The formation of a metal jet is proposed to be advantageous for the fracturing of the oxide layers that cover a powder and a substrate, as well as a means of enabling true metal to metal contact to be established [3,11].

The bonding of cold-sprayed powder with substrate is highly influenced by powder's plastic deformation, and consequently, various studies have investigated the bonding mechanism by depositing various powder materials with different properties onto different substrates [3,5–7,11–18]. Kim et al. [16] studied bonding mechanisms by examining the recrystallization phenomenon associated with a cold-sprayed titanium coating onto three different substrates (i.e., titanium, aluminum, and zirconia), and various dynamic recrystallization behaviors and interface features were reported. Meng et al. [17] proposed layered powder/substrate and crater powder models for material systems in which the powder and substrate exhibit considerably different deformability (i.e., soft powder (Al)/hard substrate (Cu) and hard powder (Cu)/soft substrate (Al) systems, respectively) in numerical simulations and have metallurgical and mechanical interlocking bonding mechanisms, respectively. Hussain et al. [18] reported that performing various substrate treatments prior to cold spraying a Cu coating exerts various effects on the dominant bonding mechanism. These effects can be attributed to metallurgical and/or mechanical interlocking mechanisms. Hussain et al. further discovered that mechanical interlocking usually accounts for a large proportion of total bonding strength; however, metallurgical bonding only contributed substantially when the AA6082 aluminum alloy substrate was polished and annealed prior to cold spraying.

Four methods are used to commercially produce metal powder for industrial applications, namely, the chemical method, the electrolytic method, the mechanical method, and atomization. Metal powders produced through these four methods differ in terms of properties such as powder size distribution, morphology, oxidation, and flow characteristics [19]. Commercial Cu feedstocks are commonly fabricated through electrolysis (EP) and atomization. Cold-sprayed Cu coatings have potential applications in power electronics [20] and pin fin array heat sinks [21]. In our previous study, three commercially available Cu feedstocks, fabricated through EP, gas-assisted water atomization (WA), and inert gas atomization (GA) processes, were characterized and cold sprayed as coatings. The original features of the powder plasticity of these three Cu powders, as demonstrated through their grain structure and plastic microstrain distribution, caused different thermomechanical reactions upon their impact with AA6061 aluminum alloy substrates and thus resulted in various coating microstructures [22]. The factors that influence the powder plasticity of Cu upon impact with a substrate include the velocity [5,15,23], temperature [8,24–26], morphology [27–29], and strain state [22] of the powder feedstock. The relationship of velocity, temperature, and morphology of Cu feedstocks with the coating microstructure and thus the bonding mechanisms has been reported in aforementioned studies. However, the microstrain of the Cu feedstocks, which significantly determine the plasticity, and its influence on the microstructure and bonding strength of cold-sprayed coating are rarely studied. In the present study, the three Cu feedstocks, which were fabricated through EP, gas-assisted WA, and inert GA processes, were characterized before and after annealing, and then cold sprayed as coatings. The influences of various thermomechanical reactions (originating from the different forms of dynamic recrystallization (plastic deformation) of the powder feedstocks upon impact) on the bonding strength of the cold-sprayed coatings on AA6061 aluminum alloy substrates are discussed herein, accompanied by the demonstration of microstrain both in Cu feedstocks and cold-sprayed coatings.

## 2. Materials and Methods

### 2.1. Cu Feedstocks and Annealing

The Cu powders used in the present study were fabricated through EP (JX Nippon Mining & Metals, Tokyo, Japan), gas-assisted WA (Fukuda Metal Foil & Powder, Kyoto, Japan), and inert GA (Thintech Materials Technology, Kaohsiung, Taiwan). The powder size distributions of the feedstocks were determined through laser diffraction (Malvern Mastersizer 2000, Malvern, UK). The morphologies of the Cu powders were inspected through scanning electron microscopy (SEM; Hitachi S3000N, Tokyo, Japan). The Cu powders were annealed for 30 min at 500 °C in a vacuum before cold spraying process. The purpose of this procedure was to further elucidate the differences in the thermomechanical properties of the EP, WA, and GA powders and the effects of annealing-induced microstructural changes on the bonding strength of cold-sprayed coatings.

### 2.2. Cold-Sprayed Cu Coatings

The PCS-1000 (Plasma Giken, Osato-gun, Japan) cold spray system was used in the present study. The Cu powders were introduced through N<sub>2</sub> carrier gas into the high-pressure chamber of a converging–diverging de Laval-type nozzle and accelerated in a supersonic stream of N<sub>2</sub> inert gas, which was preheated to 600 °C and controlled at 5 MPa. In the present study, the combined effects of velocity and temperature on the plasticity of the Cu powders were assumed to be equivalent under a given set of cold spray parameters. We adopted cold spray parameters sufficient for accelerating Cu feedstocks above the critical velocity of 570 m/s [5,15,23]. The substrate used in the cold spraying experiment was an AA6061 aluminum alloy substrate with the dimensions of 100 (length) × 100 (width) × 3 (thickness) mm<sup>3</sup>. The standoff distance was set to 30 mm. The original and annealed Cu powders were cold sprayed as coatings onto the AA6061 substrates. The cold-sprayed coatings produced from the original EP, WA, and GA powders were denoted as the OEP, OWA, and OGA coatings, respectively; the cold-sprayed coatings produced from annealed EP, WA, and GA powders were denoted as the AEP, AWA, and AGA coatings, respectively. The cross-section specimens for measuring Vickers hardness (HV0.1) were cut from the cold-sprayed Cu-coated AA6061 substrates and mounted in thermosetting resin (Buehler KonductoMet, Lake Bluff, IL, USA), after which they were ground and polished. The hardness of a cold-sprayed Cu coating was measured using the Mitutoyo Hardness Testing Machine HM, Kawasaki, Japan.

The bonding strength of the cold-sprayed Cu coating was measured according to the standard test method of ASTM C633 using a tensile test machine. Discs of cold-sprayed Cu-coated AA6061 substrate with a 1 in diameter and 3 mm thickness were cut using a wire saw from 100 (length) × 100 (width) × 3 (thickness) mm<sup>3</sup> plates that have Cu coatings thereon with a nominal thickness of 150 µm. To prepare tensile specimens, two steel rods (each rod having a 1 in diameter and 55 mm length) were grit-blasted by Al<sub>2</sub>O<sub>3</sub> particles to roughen and clean the end surfaces. Each cold-sprayed Cu-coated AA6061 disc was affixed between the clean-end surfaces of the two rods by using a heat-cured epoxy (3M Scotch-Weld 2214, St. Paul, MN, USA). The adhesion and curing of the components were conducted under pressure in a fixture at 190 °C for 2 h. The completed specimens were then subjected to the tensile test at a constant crosshead speed of 0.02 mm/s until failure. The bonding strength measurements for each type of testing material and treatment were performed on eight specimens ( $n = 8$ ), and the bonding strength data were reported as means and standard deviations.

### 2.3. Microstructure Analysis

The electron back-scattered diffraction (EBSD) technique was applied to analyze the grain structure and plastic microstrain within the powders and coatings. Field-emission SEM (FESEM; Zeiss Supra 55 equipped with an Oxford Nordlys EBSD detector, Jena, Germany) was used to obtain secondary electron images and EBSD data. The scan step sizes of 15 or 30 nm were used for EBSD measurements, and the electron beam conditions of

20 kV and 10 nA were applied for the FESEM-based analysis. The cross-section specimens for the EBSD analysis were cut from cold-sprayed Cu-coated AA6061 substrates and mounted in KonductoMet thermosetting resin. Similarly, the Cu powder specimens for the EBSD analysis were first mixed with KonductoMet resin powder and then mounted after undergoing a thermosetting process. The mounted specimens were grounded with SiC paper with a grit up to 1500 and then polished using a 1  $\mu\text{m}$  MicroPolish II suspension (Buehler, Lake County, IL, USA) and 0.25  $\mu\text{m}$  MasterPolish suspension (Buehler, Lake County, IL, USA). The specimens were further polished using a Leica EM TIC 3X Ion Beam Milling System (Wetzlar, Germany) with a beam size of 0.8 mm, voltage level of 8 kV, and current level of 3 mA. For FESEM EBSD analysis, all the mounted specimens were tilted at 70° and kept at a working distance of 12 or 14 mm.

### 3. Results

#### 3.1. Microstructures and Mechanical Properties of Cu Powders

##### 3.1.1. Morphology

The EP, WA, and GA powders were fabricated through EP, gas-assisted WA, and inert GA, respectively. The powder size distributions and morphologies are reported to have effects on the velocity and temperature of powder feedstocks upon impact substrates [8,15,26–28]. The results for the powder size distributions of these three Cu powders are listed in Table 1, revealing that the WA powder had the smallest powder size. SEM-attained morphologies of the EP, WA, and GA powders are presented in Figure 1a–c, respectively. The morphology of the EP powder (Figure 1a) exhibits a dendritic structure and irregular shape; by contrast, the WA (Figure 1b) and GA (Figure 1c) powders have near-spherical and spherical shapes, respectively.

**Table 1.** Properties of original and annealed electrolyzed powder (EP), gas-assisted water-atomized (WA) powder, and gas-atomized (GA) powder: morphology, powder size distributions, and percentages of misorientations within grains when angles are  $>1.5^\circ$  in kernel average misorientation (KAM).

Powders	EP		WA		GA	
	Original	Annealed	Original	Annealed	Original	Annealed
Morphology	Dendritic		Near-spherical		Spherical	
Powder size D <sub>10</sub> /D <sub>50</sub> /D <sub>90</sub> ( $\mu\text{m}$ )	10/30/67	–	7/11/20	–	17/40/79	–
% KAM ( $>1.5^\circ$ )	2.3%	0%	0.5%	0.3%	2.3%	0%

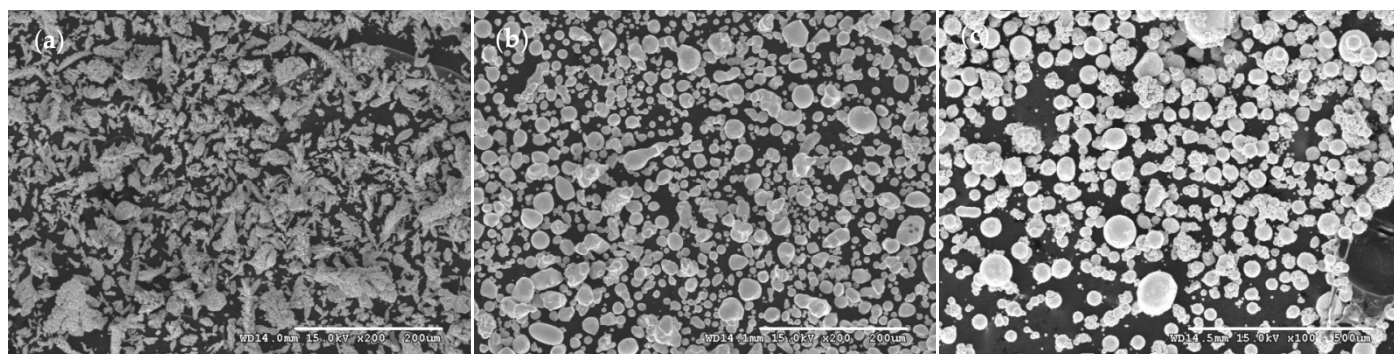


**Figure 1.** Scanning electron microscopy morphologies of (a) electrolyzed, (b) gas-assisted water-atomized, and (c) gas-atomized Cu powders.

### 3.1.2. Grain Structure and Strain State

The plasticity of powder can be characterized by the grain structure and strain state. The grain structure and plastic microstrain within the powders before and after annealing were analyzed through EBSD, and the results were presented as grain boundary (GB) and kernel average misorientation (KAM) data. The GBs were resolved and classified as the oriented angles of  $>15^\circ$ ,  $5^\circ$ – $15^\circ$ , and  $1^\circ$ – $5^\circ$ . The secondary electron (SE) images of the original EP, WA, and GA powders mounted in thermosetting resins are shown in Figure 2a,c,e, respectively, and the corresponding areas analyzed by subsequent EBSD are indicated by circular lines. The KAM + GB maps of the original EP, WA, and GA powders are illustrated in Figure 2b,d,f, respectively. The analysis results reveal that the individual particles of EP, WA, and GA powders are polycrystalline and most GBs have angles greater than  $5^\circ$ . The local crystallographic misorientation or subgrain features within grains can be recognized as the plastic microstrain [30]. The KAM technique was used to reveal the plastic microstrain of the Cu powders represented by local crystallographic misorientation. A scan step size of 15 nm was used to acquire sufficient data to perform a KAM analysis. Plastic microstrain refers to the deformation state of a powder's grain, and it can influence the microstructure of a cold-sprayed coating that has suffered intensive plastic deformation. In the KAM legend in Figure 2, the green area indicates high local misorientation with the angles  $0.8^\circ$ – $2.6^\circ$  relative to the blue area with angles of  $<0.8^\circ$  (see the bottom section of Figure 2b,d,f). KAM values of  $>1.5^\circ$  were summarized and normalized to the total KAM, and the resultant data are listed as proportional percentages in Table 1. The high angles of local misorientation within the grains of an individual powder indicate the presence of severe strain. All the EP, WA, and GA powders exhibited inherited strain from manufacturing processes; nevertheless, for the percentages of the local misorientation within grains with angles of  $>1.5^\circ$ , those of the EP (2.3%) and GA (2.3%) powders were similar, and that of the WA powder (0.5%) was the smallest (Table 1). The results were also consistent with our previous study [22].

The annealed Cu powders were also analyzed by EBSD. The SE images and the corresponding areas analyzed through the EBSD KAM + GB mapping of the annealed EP, WA, and GA powders are presented in Figure 3a–f, respectively. The recrystallization and grain growth phenomena of the annealed Cu powders were assessed by comparing the KAM + GB maps of the annealed Cu powders with those of the original powders (see Figure 2b,d,f and Figure 3b,d,f). The KAM + GB maps presented in Figure 3b,d,f reveal that the local misorientations with high angles of  $0.8$ – $2.6^\circ$  (the green area) almost disappeared. These maps also reveal that the strain release in the grains, as indicated by the blue area ( $<0.8^\circ$ ) and the presence of low-angle ( $1$ – $5^\circ$ ) grain boundaries. The aforementioned phenomena are not observed in Figure 2b,d,f, in contrast to the annealing effect. The recrystallization of Cu into a twin-grain structure has been reported by other studies [31–33], and this phenomenon is also observed in the annealed EP and GA powders (Figure 3b,f) examined in the present study. However, the grains of the annealed WA powder were not recrystallized into a twin-grain structure but into equiaxed grains instead. The amount of local misorientation with angles of  $>1.5^\circ$  within the grains of the annealed EP, WA, and GA powders was also calculated and is presented as percentage values in accordance with the respective KAM legends in Figure 3b,d,f. Table 1 also lists the analysis results, revealing that the changes in the  $>1.5^\circ$  misorientation (presented as percentage values) within the grains of the EP, WA, and GA powders before and after annealing were 2.3% to 0%, 0.5% to 0.3%, and 2.3% to 0%, respectively. The plastic microstrain remaining in the original Cu grains (Figure 2b,d,f) was released after annealing through recrystallization and grain growth (Figure 3b,d,f). The twin boundaries exhibited by the annealed EP and GA powders may influence powder plasticity [33].

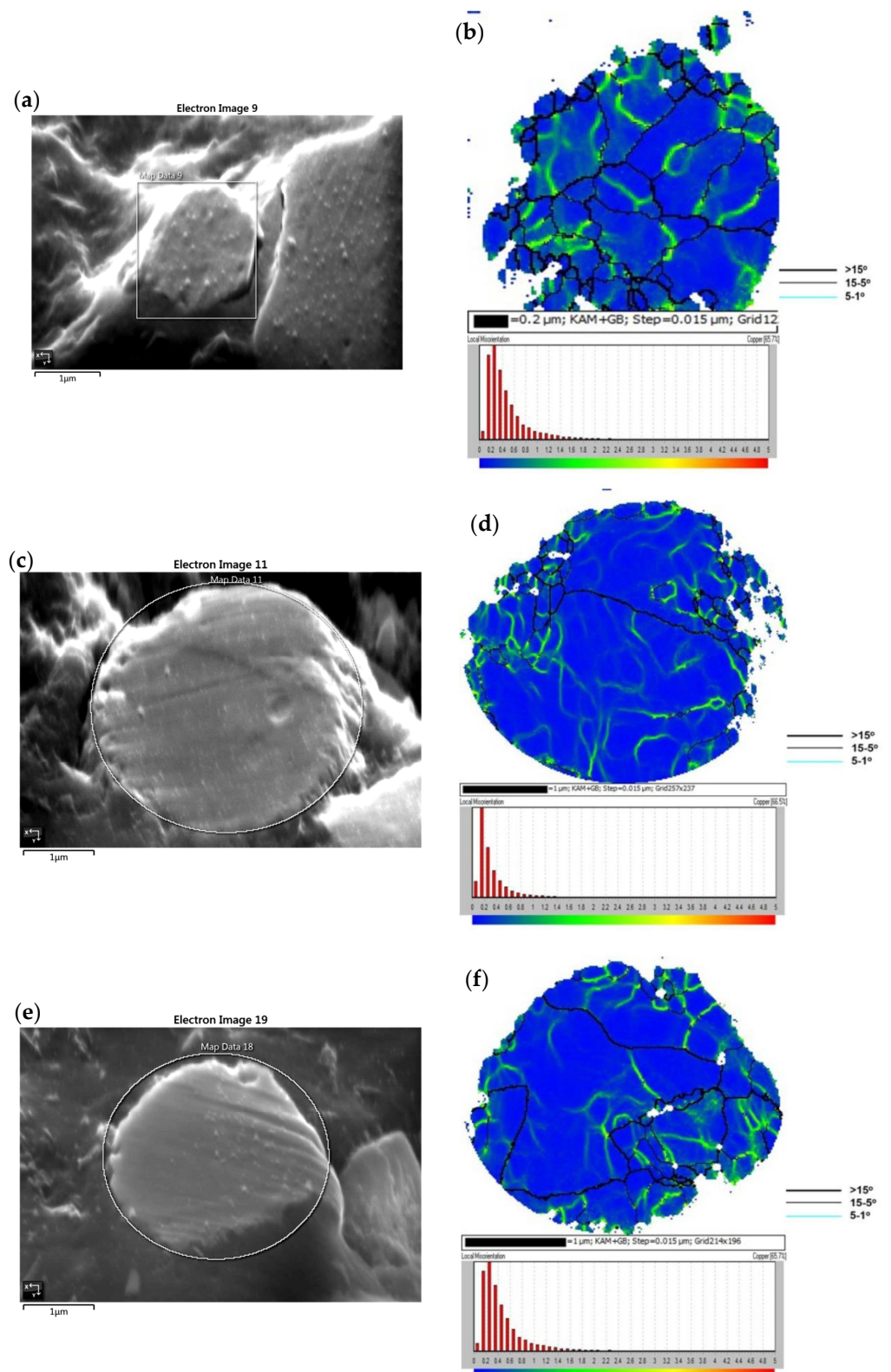


**Figure 2.** Secondary electron images and corresponding kernel average misorientation (KAM) + grain boundary (GB) maps of original Cu powders produced through various processes: (a,b), electrolyzed powders; (c,d), gas-assisted water-atomized powders; (e,f), gas-atomized powders.

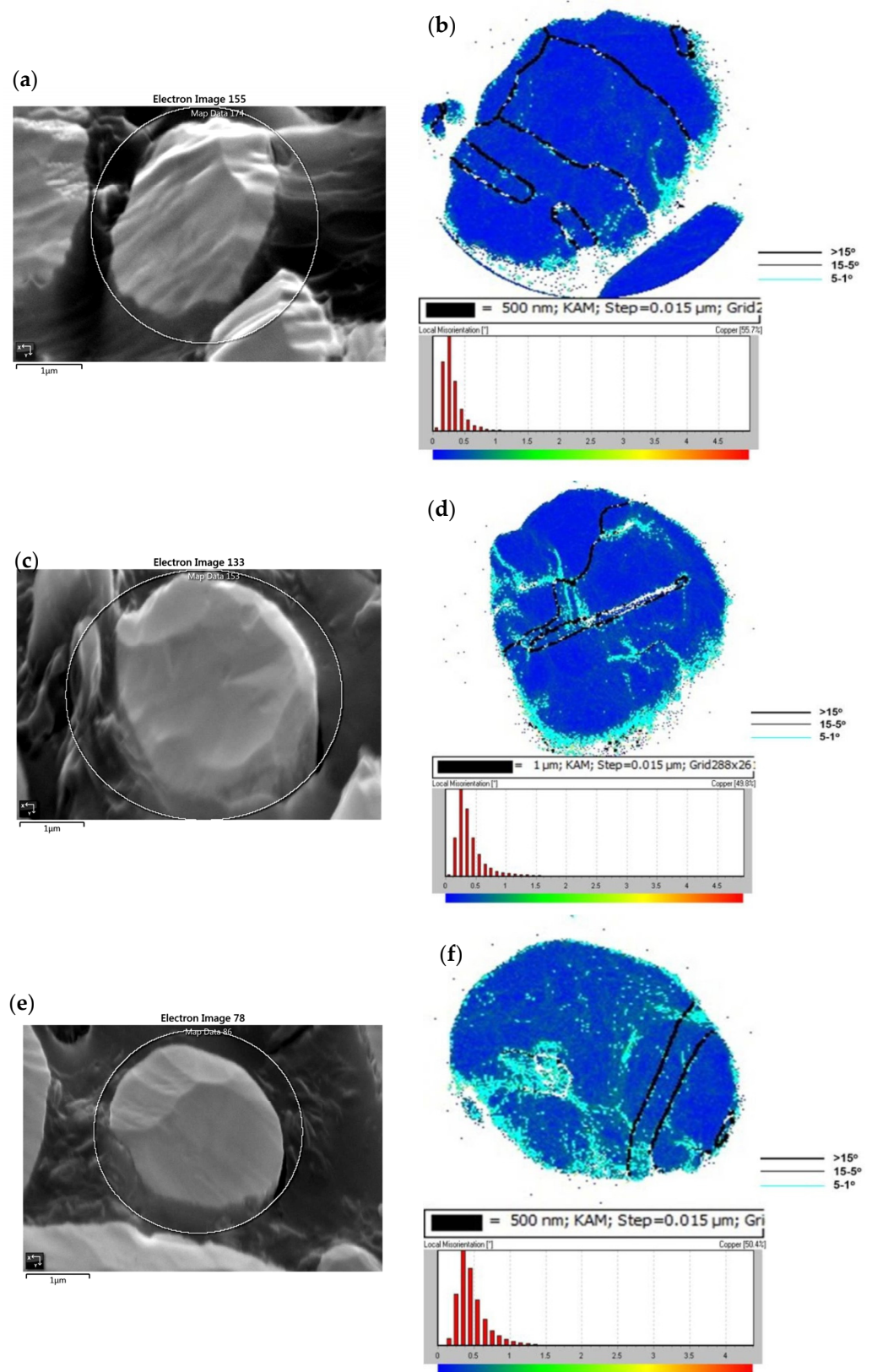


**Figure 3.** Secondary electron images and corresponding kernel average misorientation (KAM) + grain boundary (GB) maps of annealed Cu powders produced through various processes: (a,b), electrolyzed powder; (c,d), gas-assisted water-atomized powder; (e,f), gas-atomized powders.

### 3.2. Microstructures and Mechanical Properties of Cold-Sprayed Coatings

#### 3.2.1. Hardness and Bonding Strength

The measured Vickers hardness (HV0.1) values of the cold-sprayed Cu coatings, which can reveal the deformation hardening effect during cold spray deposition, made from original and annealed feedstock powders are listed in Table 2. All the coatings made from annealed powders (i.e., the AEP, AWA, and AGA coatings) have lower hardness values than those made from original powders (i.e., the OEP, OWA, and OGA coatings). The lower hardness and thus lower deformation hardening of the AEP, AWA, and AGA coatings may be due to the improved plasticity of the annealed EP, WA, and GA powders, achieved through strain release and grain growth in addition to the appearance of low-angle ( $1^{\circ}$ – $5^{\circ}$ ) GBs. Table 2 also reveals that the bonding strength levels of the AEP, AWA, and AGA coatings were higher than those of the OEP, OWA, and OGA coatings. It represents that the AGA coating had the most significant improvement in bonding strength with a value of  $45.6 \pm 3.2$  MPa and an increment ratio of 1.98 compared with the OGA coating.

**Table 2.** Properties of cold-sprayed coatings produced from original electrolyzed powder (OEP), gas-assisted water-atomized powder (OWA), and gas-atomized powder (OGA), and from respective annealed powders (AEP, AWA, and AGA): Vicker’s hardness (HV0.1), bonding strength, and percentages of misorientations within grains when angles are  $>1.5^{\circ}$  in kernel average misorientation (KAM) legend.

Coatings	OEP	AEP	OWA	AWA	OGA	AGA
Hardness (HV0.1)	154	120	156	119	136	105
Bonding strength (MPa)	$8.0 \pm 0.7$	$11.3 \pm 1.8$	$12.0 \pm 1.5$	$21.3 \pm 4.4$	$23.0 \pm 2.4$	$45.6 \pm 3.2$
% KAM ( $>1.5^{\circ}$ )	1.2%	0.7%	3.0%	0.5%	1.5%	0%

#### 3.2.2. Grain Structure and Strain State

The grain structure and plastic strain distribution of the cold-sprayed coating located close to the coating–substrate interface are presented as EBSD Euler contrast and KAM + GB maps, respectively. For EBSD measurements, the normal direction of the polished plane of a cross-section specimen is represented as the z-axis of the EBSD coordinate system. Accordingly, the impact direction of the cold spray is parallel to the y-axis. The Euler contrast and KAM + GB maps of the cold-sprayed OEP, OWA, and OGA coatings are presented in Figure 4a–f, respectively. The Euler contrast maps reveal clear grain structures, and the recrystallization of Cu near the coating/substrate interface is observed in the OEP, OWA, and OGA coatings, which are shown in Figure 4a,c,e, respectively. Notably, in the OEP (Figure 4a) and OGA (Figure 4e) coatings, the recrystallization of Cu is characterized as a twin GB; this phenomenon is not observed in the OWA coating (Figure 4c). The Cu powder produced through gas-assisted WA and the subsequent cold-sprayed Cu coating appear to be preferably recrystallized as equiaxed grains. Furthermore, the OGA coating (Figure 4e) appears to have a greater tendency to develop recrystallized twin grains than the OEP coating, which exhibits more new grains that are recrystallized as equiaxed grains instead of twin grains (Figure 4a). According to the KAM + GB maps of the cold-sprayed OEP, OWA, and OGA coatings, as shown in Figure 4b,d,f, respectively, the percentages of local misorientations with angles of  $>1.5^{\circ}$  within the grains were calculated, and the results are listed in Table 2. As indicated in Table 2, the OEP and OGA coatings exhibited more strain release relative to the OWA coating because the percentages of misorientations with angles of  $>1.5^{\circ}$  within the grains in the OEP (1.2%) and OGA (1.5%) coatings were approximately equivalent and smaller than those in the OWA coating (3.0%). Even though the cold-sprayed OEP and OGA coatings had a similar strain release, the hardness of the OGA coating was less than that of the OEP coating (Table 2). The plasticity of Cu can be



improved by the occurrence of deformation twins [33]. The OGA coating had a greater tendency to have recrystallized twin grains than did the OEP coating, which appears to explain the lower hardness of the OGA coating relative to the OEP coating. Among the OEP, OWA, and OGA coatings, the cold-sprayed OWA coating had the highest percentage of misorientations, with angles of  $>1.5^\circ$ , but did not exhibit a considerable increase in hardness. This phenomenon may be due to the lower level of strain that accumulated in the WA powder (0.5% in Table 1), which resulted in fewer tangled dislocations after the cold spraying process for the WA powder.

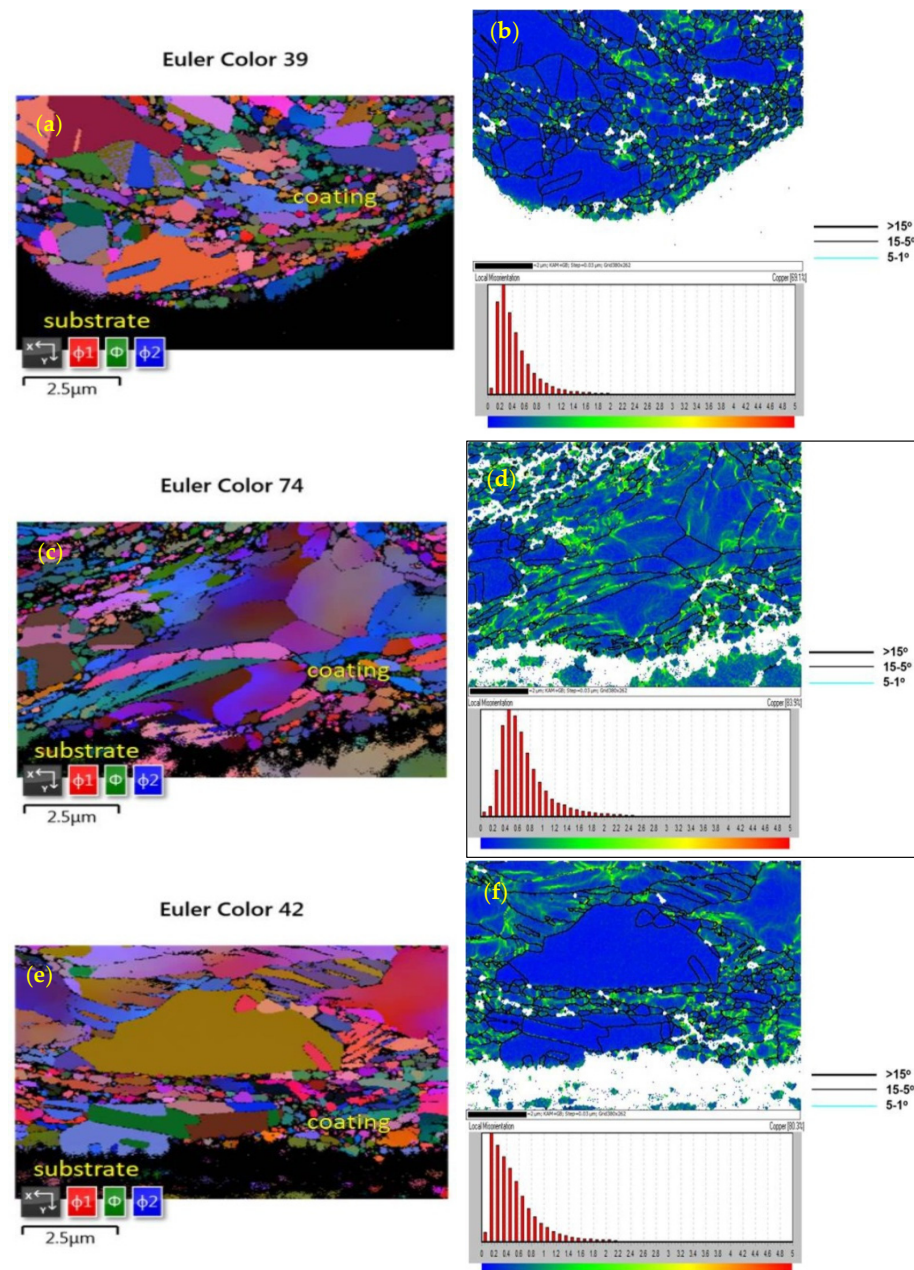


**Figure 4.** Euler contrast and kernel average misorientation (KAM) + grain boundary (GB) maps of cold-sprayed OEP (a,b), OWA (c,d), and OGA coatings (e,f), recorded at the coating–substrate interface.

The EBSD Euler contrast and KAM + GB maps of the cold-sprayed AEP, AWA, and AGA coatings made from the annealed EP, WA, and GA powders are presented in Figure 5a–f, respectively. The percentages of misorientations with angles of  $>1.5^\circ$  within the grains of the AEP, AWA, and AGA coatings were also calculated on the basis of the

KAM + GB maps in Figure 5b,d,f, respectively, and the results are listed in Table 2. Notably, the Euler contrast maps in Figure 5a,c,e reveal that the cold-sprayed AEP, AWA, and AGA coatings generally exhibit well-recrystallized grains and strain release even after intensive deformation upon impact; furthermore, this phenomenon is most prominent in the AGA coating. The percentages of misorientations with angles of  $>1.5^\circ$  within the grains in the AEP (0.7%), AWA (0.5%), and AGA coatings (0%) were low (Table 2); this finding is consistent with the occurrence of well-recrystallized grains in the Euler contrast maps of the AEP (Figure 5a), AWA (Figure 5c), and AGA (Figure 5e) coatings and the lower hardness of the AEP, AWA, and AGA coatings relative to the OEP, OWA, and OGA coatings (Table 2).

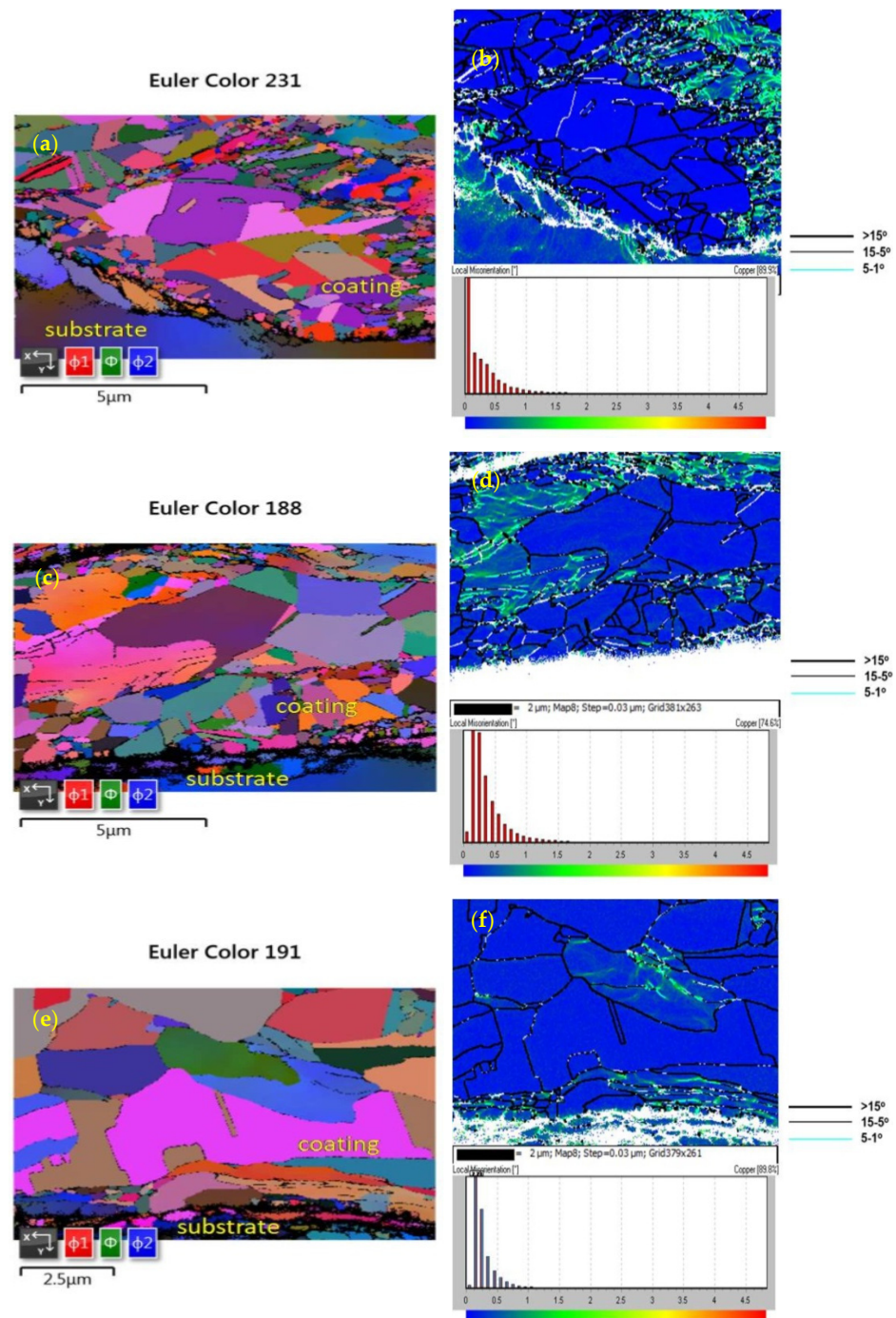


**Figure 5.** Euler contrast and kernel average misorientation (KAM) + grain boundary (GB) maps of cold-sprayed AEP (a,b), AWA (c,d), and AGA coatings (e,f), recorded at the coating–substrate interface.

## 4. Discussion

The specimen preparation for EBSD analysis was carried out carefully to minimize any residual surface deformation introduced during grinding and polishing, which can affect background correction and band detection. Etchants which preferentially attack grain boundaries were also avoided. In addition to traditional SiC grinding paper and polish suspension for specimen preparation, ion beam milling was adopted to ensure the quality of EBSD patterns in the present study [34].

### 4.1. Powder Plasticity

Generally, small powders are easily accelerated to high velocities [14]. However, the critical velocity of a powder greatly depends on powder temperature and it increases with decreasing powder temperature [8,26]. T. Schmidt et al. reported that the larger Cu powder (50  $\mu\text{m}$ ) has significantly higher powder temperature than the smaller one (5  $\mu\text{m}$ ), with a value of 140  $^{\circ}\text{C}$  in numerical simulation [14]. The significant effect of powder temperature (critical velocity) on the plastic deformation of powder upon impact is also simulated and reported in some studies [24,25]. Consequently, in the present study, the combined effects of velocity and temperature on the plasticity of the Cu powders were assumed to be equivalent under a given set of cold spray parameters. Notably, the property changes in the original powders after undergoing annealing were revealed to have distinctive effects on the microstructures of cold-sprayed coatings. The annealing treatment of the EP, WA, and GA powders were demonstrated to have effects on strain release and low GB angle with respect to the original powders because of recrystallization and grain growth. The angles of the GBs of the original powders were greater than those of the annealed powders even though the microstrains were low, as evident in the original WA powder (0.5%), and the consequent microstrains in the OEP (1.2%), OWA (3.0%), and OGA (1.5%) coatings were higher than those in the AEP (0.7%), AWA (0.5%), and AGA (0%) coatings after cold spraying. Therefore, the strain release and low GB angle of the annealed powders were inferred to be responsible for the formation of recrystallized ductile coatings after cold spraying. Furthermore, the hardness of Cu (approximately 350 HV) is typically higher than that of AA6061 (approximately 100 HV). Several studies have discussed the bonding mechanism of cold-sprayed Cu coating on Al substrate. A study conducted a numerical simulation and reported that the penetration of hard Cu powder into soft Al substrate contributes the bonding mechanism of mechanical interlocking in addition to plastic recrystallization [17], which is regarded as the foundation for the triggering of a metallurgical bonding mechanism [6,8–10]. Schmidt et al. [14] discussed the key role of powder mechanical properties in predicting powder bonding during cold spraying, and they proposed the taking of hardness measurements at the cross-section of a powder for use in predictions. Hussain et al. [18] demonstrated that the mechanical interlocking of cold-sprayed Cu coating and AA6082 substrate materials accounts for a large proportion of total bonding strength. The higher plasticity of the annealed EP, WA, and GA powders (relative to the original powders) because of their strain release and low GB angle may help the viscous flow of Cu powder to penetrate more deeply into the AA6061 substrate under a given set of cold spray parameters. Therefore, a viscous flow leads to the formation of a metal jet consisting of Cu and AA6061 materials, and thus, the mechanical interlocking may be more effective for the cold spraying of annealed Cu powder. In the present study, the bonding strength levels of the cold-sprayed AEP, AWA, and AGA coatings made from the annealed EP, WA, and GA powders, respectively, were generally higher than those of the OEP, OWA, and OGA coatings made from the original powders (Table 2). No evidence of a metal jet consisting of Cu and AA6061 located close to the coating–substrate interfaces of the AEP, AWA, and AGA coatings was revealed through the microstructural EBSD investigation, and this is a topic that requires further clarification. However, the improved powder plasticity that resulted from the strain release and the low GB angle achieved through annealing appears to be beneficial for both metallurgical and mechanical interlocking bonding mechanisms.

The bonding strength of the OEP coating was considerably less than that of the OGA coating (Table 2) even when the microstrains were similar to those of the original powders (2.3% for both powders) and the coatings (1.2% for OEP coating and 1.5% for OGA coating) after cold spraying. In addition to the microstrain factor, the factors influencing powder plasticity upon the impact of a powder with a substrate include velocity [15], temperature [8,26], and morphology [27,28]. In the present study, the combined effects of velocity [15,27,28] and temperature [8,26] on the plasticity of the Cu powders were assumed to be equivalent under a given set of cold spray parameters. Therefore, the morphology of the original EP powder with a dendritic structure was inferred to be responsible for the lower bonding strength of the OEP coating than OGA coating. In one study [27], Cu powders produced through EP and GA were used to prepare cold-sprayed coatings, and the irregular dendritic structure of the EP powder in that study was reported as the reason for the Archimedes porosity of the resulting EP coating being higher than that of the resulting GA coating. Accordingly, the asymmetric dendritic morphology of EP powder was inferred not to be conducive to the intensive plastic deformation that determines the bonding strength of cold-sprayed coating. This reasoning can also be applied to explain the difference in the bonding strength levels of the AEP and AGA coatings.

In our previous study [22], the OWA coating was the only one that exhibited a jet-forming coating structure under metallographic microscopy; it consequently had the highest microstrain out of all tested coatings. The WA powder, which had the smallest powder size among the EP, WA, and GA powders, should have the lowest powder temperature among the three powders as it streams out of the cold spray nozzle [14]. This phenomenon increases the critical velocity of the WA powder [8,26] and limits plastic deformation and recrystallization upon impact. By contrast, the strain release and ductility of the OGA coating (Table 2), which has a 1.5% microstrain and a recrystallized twin-grain structure, result in the coating having a higher bonding strength relative to the OWA coating. Thus, the well-recrystallized structure of a cold-sprayed Cu coating is inferred to have the effect of enhancing bonding strength; however, having less recrystallization and the formation of a residual jet-forming structure do not have the same effect, even though a jet-forming structure is usually regarded as a representation of intensive plastic deformation [5–7].

#### 4.2. Recrystallized Twin Grains

Notably, recrystallized twin grains were observed in the OEP and OGA coatings and the annealed EP and GA powders. Under the similar microstrain conditions of OEP (1.2%) and OGA (1.5%) coatings, it can be recognized that twin grains were more well-recrystallized in the OGA coating (Figure 4e) than in the OEP coating (Figure 4a). Similar results were also shown in our previous study [22]. Twin grains that directly recrystallize through a rotational mechanism because of high-strain-rate deformation during or shortly after impact are arranged in characteristic parallel arrays, whereas twin grains that are formed through migration during the subsequent annealing that occurs in the cooling period following adiabatic strain heating are not arranged in the aforementioned pattern [35]. In the present study, the twins in the OGA coating (Figure 4e) did not have prominent parallel arrays [22]; however, the occurrence of migration twins was more prominent in the OGA coating (Figure 4e) than in the OEP coating (Figure 4a).

The microstrains in the annealed EP and GA powders were 0% and released as recrystallized twin grains, but those in the annealed WA powder were 0.3% and recrystallized as equiaxed grains. The twin grains in the annealed EP and GA powders are expected to be beneficial for plastic deformation upon impact during cold spraying. The higher bonding strength of the AGA coating relative to the AEP and AWA coatings demonstrated that the influencing factors of the powder plasticity include not only strain release and the angles of low GBs but also having a spherical shape and recrystallized twin grains. Table 2 reveals that the cold-sprayed Cu coatings prepared from annealed powders generally have lower levels of hardness relative to those made from the original powders. The greater strain release and ductility of the AEP, AWA, and AGA coatings relative to the OEP, OWA, and

OGA coatings indicate that dynamic recrystallization is essential for improving bonding strength. The homogeneous microstructure of the spherical Cu feedstocks may be induced by strain release, recrystallized twin grains, and grain growth (low-angle boundaries) through annealing such that cold-sprayed Cu coatings exhibit improved ductility and reduced hardness. This finding indicates that the cold-sprayed coatings have less strain hardening and residual stress, which are regarded as key advantages for bonding strength.

## 5. Conclusions

Three copper feedstocks fabricated through EP, gas-assisted WA, and inert GA processes were characterized and annealed before cold spraying. The thermomechanical reactions of sprayed powders with AA6061 substrates and their effects on the bonding strength of coatings were assessed by examining grain structures and the microstrain of powders and corresponding coatings. The following conclusions are summarized based on our results and discussion:

1. The plasticity of Cu powder is improved through strain release and low GB angle after annealing treatment at 500 °C for 30 min. This plasticity plays a role in increasing the bonding strength of cold-sprayed coatings, characterized by an excellent dynamic recrystallization structure and a bonding strength increment ratio up to 1.98.
2. The Cu powders with an asymmetric dendritic morphology are detrimental for intensive plastic deformation, which results in the lowest bonding strength ( $8.0 \pm 0.7$  MPa) of cold-sprayed coating.
3. Recrystallized twin grains are beneficial for plasticity, and they can help increase the bonding strength of cold-sprayed coatings.

**Author Contributions:** Conceptualization, experiment, writing—original draft preparation, F.-J.W.; Methodology, investigation, B.-Y.C.; Supervision, K.-Z.F.; Writing—review and editing, S.-Y.T. and C.-W.Y. All authors have read and agreed to the published version of the manuscript.

**Funding:** This research received no external funding.

**Institutional Review Board Statement:** Not applicable.

**Informed Consent Statement:** Not applicable.

**Data Availability Statement:** No new data were created or analyzed in this study. Data sharing is not applicable to this article.

**Conflicts of Interest:** The authors declare no conflict of interest.

## References

1. Mohammadpour, E.; Liew, W.Y.H.; Radevski, N.; Lee, S.; Mondinos, N.; Altarawneh, M.; Minakshi, M.; Amri, A.; Rowles, M.R.; Lim, H.N.; et al. High temperature (up to 1200 °C) thermal-mechanical stability of Si and Ni doped CrN framework coatings. *J. Mater. Res. Technol.* **2021**, *14*, 2406–2419. [[CrossRef](#)]
2. Papyrin, A.N.; Kosarev, V.F.; Klinkov, S.; Alkhimov, A.P.; Fomin, V. *Cold Spray Technology*; Elsevier: Amsterdam, The Netherlands, 2007.
3. Alkhimov, A.P.; Papyrin, A.N.; Kosarev, V.F.; Nesterovich, N.I.; Shuspanov, M.M. Gas-Dynamic Spraying Method for Applying a Coating. U.S. Patent No. 5,302,414, 12 April 1994.
4. Voyer, J.; Stoltenhoff, T.; Kreye, H. Development of Cold Sprayed Coatings. In *Thermal Spray 2003: Advancing the Science and Applying the Technology, Proceedings of the 2003 International Thermal Spray Conference, Orlando, FL, USA, 5–8 May 2003*; Marple, B.R., Moreau, C., Eds.; ASM International: Almere, The Netherlands, 2003; pp. 71–78.
5. Stoltenhoff, T.; Kreye, H.; Richter, H.J. An analysis of the cold spray process and its coatings. *J. Therm. Spray Technol.* **2002**, *11*, 542–550. [[CrossRef](#)]
6. Assadi, H.; Gärtner, F.; Stoltenhoff, T.; Kreye, H. Bonding mechanism in cold gas spraying. *Acta Mater.* **2003**, *51*, 4379–4394. [[CrossRef](#)]
7. Schmidt, T.; Gärtner, F.; Assadi, H.; Kreye, H. Development of a generalized parameter window for cold spray deposition. *Acta Mater.* **2006**, *54*, 729–742. [[CrossRef](#)]
8. Grujicic, M.; Zhao, C.L.; DeRosset, W.S.; Helfritch, D. Adiabatic shear instability based mechanism for particles/substrate bonding in the cold-gas dynamic-spray process. *Mater. Des.* **2004**, *25*, 681–688. [[CrossRef](#)]

9. Dykhuizen, R.C.; Smith, M.F.; Gilmore, D.L.; Neiser, R.A.; Jiang, X.; Sampath, S. Impact of high velocity cold spray particles. *J. Therm. Spray Technol.* **1999**, *8*, 559–564. [[CrossRef](#)]
10. Li, W.Y.; Liao, H.L.; Li, C.J.; Bang, H.S.; Coddet, C. Numerical simulation of deformation behavior of Al particles impacting on Al substrate and effect of surface oxide films on interfacial bonding in cold spraying. *Appl. Surf. Sci.* **2007**, *253*, 5084–5091. [[CrossRef](#)]
11. Champagne, V.K. *The Cold Spray Materials Deposition Process: Fundamentals and Applications*; CRC: Cambridge, UK, 2007.
12. Gilmore, D.L.; Dykhuizen, R.C.; Neiser, R.A.; Smith, M.F.; Roemer, T.J. Particle velocity and deposition efficiency in the cold spray process. *J. Therm. Spray Technol.* **1999**, *8*, 576–582. [[CrossRef](#)]
13. Gärtner, F.; Stoltenhoff, T.; Schmidt, T.; Kreye, H. The cold spray process and its potential for industrial applications. *J. Therm. Spray Technol.* **2006**, *15*, 223–232. [[CrossRef](#)]
14. Schmidt, T.; Assadi, H.; Gärtner, F.; Richter, H.; Stoltenhoff, T.; Kreye, H.; Klassen, T. From particle acceleration to impact and bonding in cold spraying. *J. Therm. Spray Technol.* **2009**, *18*, 794–808. [[CrossRef](#)]
15. Huang, R.; Ma, W.; Fukanuma, H. Development of ultra-strong adhesive strength coatings using cold spray. *Surf. Coat. Technol.* **2014**, *258*, 832–841. [[CrossRef](#)]
16. Kim, K.; Watanabe, M.; Kuroda, S. Bonding mechanisms of thermally softened metallic powder particles and substrates impacted at high velocity. *Surf. Coat. Technol.* **2010**, *204*, 2175–2180. [[CrossRef](#)]
17. Meng, F.; Hu, D.; Gao, Y.; Yue, S.; Song, J. Cold-spray bonding mechanisms and deposition efficiency prediction for particle/substrate with distinct deformability. *Mater. Design* **2016**, *109*, 503–510. [[CrossRef](#)]
18. Hussain, T.; McCartney, D.G.; Shipway, P.H.; Zhang, D. Bonding mechanisms in cold spraying: The contributions of metallurgical and mechanical components. *J. Therm. Spray Technol.* **2009**, *18*, 364–379. [[CrossRef](#)]
19. Huppmann, W.J.; Dalal, K. *Metallographic Atlas of Powder Metallurgy*; Verlag Schmid GmbH: Freiburg, Germany, 1986.
20. Kosarev, V.F.; Klinkov, S.V.; Melamed, B.M.; Nepochatov, Y.K.; Ryashin, N.S.; Shikalov, V.S. Cold spraying for power electronics: Deposition of thick topologically patterned copper layers on ceramics. In Proceedings of the International Conference on the Methods of Aerophysical Research, Novosibirsk, Russia, 13–19 August 2018; p. 030047.
21. Perry, J.; Richer, P.; Jodoin, B.; Matte, E. Pin fin array heat sinks by cold spray additive manufacturing: Economics of powder recycling. In Proceedings of the International Thermal Spray Conference, Orlando, FL, USA, 7–9 May 2018; ASM International: Almere, The Netherlands, 2018.
22. Wei, F.J.; Chou, B.Y.; Tsai, S.Y.; Fung, K.Z. Thermomechanical properties of cold-sprayed copper coatings from differently fabricated powders. *Surf. Coat. Technol.* **2022**, *434*, 128128. [[CrossRef](#)]
23. Jakupi, P.; Keech, P.G.; Barker, I.; Ramamurthy, S.; Jacklin, R.L.; Shoosmith, D.W.; Moser, D.E. Characterization of commercially cold sprayed copper coatings and determination of the effects of impacting copper powder velocities. *J. Nucl. Mater.* **2015**, *466*, 1–11. [[CrossRef](#)]
24. Yu, M.; Li, W.Y.; Wang, F.F.; Suo, X.K.; Liao, H.L. Effect of particle and substrate preheating on particle deformation behavior in cold spraying. *Surf. Coat. Technol.* **2013**, *220*, 174–178. [[CrossRef](#)]
25. Yin, S.; Wang, X.; Suo, X.; Liao, H.; Guo, Z.; Li, W.; Coddet, C. Deposition behavior of thermally softened copper particles in cold spraying. *Acta Mater.* **2013**, *61*, 5105–5118. [[CrossRef](#)]
26. Fukanuma, H.; Ohno, N.; Sun, B.; Huang, R. In-flight particle velocity measurements with DPV-2000 in cold spray. *Surf. Coat. Technol.* **2006**, *201*, 1935–1941. [[CrossRef](#)]
27. Li, Y.J.; Luo, X.T.; Li, C.J. Dependency of deposition behavior, microstructure and properties of cold sprayed Cu on morphology and porosity of the powder. *Surf. Coat. Technol.* **2017**, *328*, 304–312. [[CrossRef](#)]
28. Li, Y.J.; Luo, X.T.; Rashid, H.; Li, C.J. A new approach to prepare fully dense Cu with high conductivities and anti-corrosion performance by cold spray. *J. Alloy. Comp.* **2018**, *740*, 406–413. [[CrossRef](#)]
29. Luo, X.T.; Ge, Y.; Xie, Y.; Wei, Y.; Huang, R.; Ma, N.; Ramachandran, C.S.; Li, C.J. Dynamic evolution of oxide scale on the surfaces of feed stock particles from cracking and segmenting to peel-off while cold spraying copper powder having a high oxygen content. *J. Mater. Sci. Technol.* **2021**, *67*, 105–115. [[CrossRef](#)]
30. Hsu, W.C.; Chang, L.; Kao, P.W. Study of potential recrystallization nuclei in the cold-rolled microstructure of an electrical steel by electron backscatter diffraction. *Mater. Sci. Eng.* **2019**, *580*, 012034. [[CrossRef](#)]
31. Borchers, C.; Gärtner, F.; Stoltenhoff, T.; Assadi, H.; Kreye, H. Microstructural and macroscopic properties of cold sprayed copper coatings. *J. Appl. Phys.* **2003**, *93*, 10064–10070. [[CrossRef](#)]
32. Feng, Y.; Li, W.; Guo, C.; Gong, M.; Yang, K. Mechanical property improvement induced by nanoscaled deformation twins in cold-sprayed Cu coatings. *Mater. Sci. Eng. A* **2018**, *727*, 119–122. [[CrossRef](#)]
33. Wang, Y.B.; Sui, M.L.; Ma, E. In situ observation of twin boundary migration in copper with nanoscale twins during tensile deformation. *Philos. Mag. Lett.* **2007**, *87*, 935–942. [[CrossRef](#)]
34. Nowell, M.M.; Witt, R.A.; True, B. EBSD sample preparation: Techniques, tips, and tricks. *Microsc. Microanal.* **2005**, *11* (Suppl. 2), 504–505. [[CrossRef](#)]
35. Murr, L.E.; Niou, C.-S.; Pappu, S.; Rivas, J.M.; Quinones, S.A. LEDs in ultra-high strain-rate deformation. *Phys. Status Solidi A* **1995**, *149*, 253–274. [[CrossRef](#)]